

Searching for Dust Reddening in SDSS Spectra with Damped Lyman α Systems

S. Frank^{1*} and C. Péroux^{1*}

¹Laboratoire d'Astrophysique de Marseille, OAMP, Université Aix-Marseille & CNRS, 38 rue Frédéric Joliot Curie, 13388 Marseille cedex 13, France

Accepted 2010 April 13. Received 2010 March 18; in original form 2009 December 07

ABSTRACT

We searched for evidence of the reddening of background QSO spectra from the Sloan Digital Sky Survey (SDSS) due to dust in intervening damped Lyman α (DLA) systems. We utilise the two Data Releases DR5 and DR7 to arrive at sample sizes of 475 (DR5) and 676 (DR7) absorbers, based on two different published lists of SDSS DLAs. Both samples span roughly the redshift range of $2.2 < z_{abs} < 5.2$, with a mean of $z \sim 3.0$, and the majority of the DLAs (75%) below $z=3.3$. We construct geometric mean spectra in the absorber restframes ranging from 1240 to ~ 2800 Å, and composite spectra of samples matching the 'DLA' QSOs in i band magnitude and emission redshift z_{em} , but without absorption lines. By comparing the slopes of these composite spectra with their matched counterparts, we find no sign of reddening in the ensemble of the absorbers from these samples. Owing to both the unprecedentedly large sizes of the DLA samples themselves and the non-DLA SDSS QSO sample, from which we can draw our matching spectra, we can place very tight limits for this non-detection ($\langle E(B-V) \rangle = -0.0013 \pm 0.0025$ (DR5) and $\langle E(B-V) \rangle = -0.0017 \pm 0.0022$ (DR7)). Interestingly, when applying our technique to the samples of York et al. (2006), vandenBerk et al. (2008) (intervening and intrinsic MgII absorbers) and the smaller DLA-subsample and pool of comparison QSOs of Vladilo et al. (2008), we do recover their results, i.e. detect the same amount of reddening as these authors do. Furthermore, we have tested whether subsamples of our large sample in categories involving the absorbers (HI column densities, presence or absence of accompanying metal absorption, absorber redshift) or the background quasars (emission redshift, brightness) do reveal dust extinction, but found no trends. These results are at odds with both detections of dust reddening from previous studies, and also with expectations from observations of high-redshift galaxies.

Key words: Quasar absorption lines - Damped Lyman alpha systems - Dust

1 INTRODUCTION

Detecting galaxies at high-redshift provides a powerful observational way to probe structure formation in the early Universe. There have now been several hundreds of galaxies found using the Lyman-break technique (e.g. Steidel et al. (1999)). Although very successful, this method is limited to luminous objects. A complementary technique to select high-redshift galaxies is the detection of systems in absorption in the spectra of background quasars. Since their selection is independent of luminosity and morphology, the study of galaxy evolution through these systems circumvents the biases inherent to traditional emission studies.

Damped Lyman- α systems (hereafter DLAs) have hydrogen column densities, $\log N(\text{HI}) > 20.3$ and are thought to be associated with parts of high-redshift galaxies, just as they are at lowest redshift (Rao et al. 2003; Chen et al. 2005). From our knowledge of the local Universe we expect that high-redshift galaxies, especially those forming stars, should contain some amount of dust. Therefore, the possibility that DLAs are dusty objects is currently hotly debated. Indeed, smoothed-particle hydrodynamic simulations (Nagamine et al. 2004) predict that DLAs should be $1/3^{\text{rd}}$ solar at $z = 2.5$ and even more metal-rich toward lower redshifts whilst current observations measure typically a metallicity around $1/10^{\text{th}}$ solar. Dust is therefore invoked to reconcile results from the simulations with current observations. In addition, one can estimate the dust content of individual DLA from the ratio of depleted onto undepleted elements it

* E-mail: sfrank@oamp.fr

contains. It is assumed that a fraction of the elements is not detected in the gas phase because it is locked into dust grains (e.g. Pettini et al. (2000)). Such studies have shown that the dust depletion levels observed in DLAs are small, lower than those measured in the Galactic interstellar-medium clouds with similar $N(\text{HI})$ column densities. In fact, the observations resemble the dust depletion of the Galactic halo warm gas (Kulkarni et al. 1997; Savaglio et al. 2000).

Another more direct way to probe the dust content of DLAs is to look for a 2175 Å feature (the so-called “dust bump”) in the quasar spectrum. This feature is known to be more predominant in the Milky Way than in the Small and Large Magellanic Clouds. Many searches lead to no-detections (Jura 1977; Smith et al. 1979; Boissé & Bergeron 1988; Lanzetta et al. 1989; Fall et al. 1989; Pei et al. 1991). Using Sloan Digital Sky Survey (SDSS) spectra, Wang et al. (2004) claimed the detections of bumps in three individual MgII absorbers at $z=1.5$, while Junkkarinen et al. (2004) have detected a clear bump in a DLA at $z=0.524$ toward a BL Lac at $z=0.94$. Other searches remained unsuccessful, indicating that most DLAs do not show a predominant 2175 Å feature. A promising tool for finding the signatures of dust are searches for the strong silicate absorption features in the infrared. Kulkarni et al. (2007), using Spitzer data, report on the first indication of 9.7 μm silicate absorption in a DLA at $z_{abs} = 0.52$, and find it to be stronger than expected from extrapolation of the relation from Galactic diffuse ISM.

A consequence of DLAs being dusty is that it might prevent the inclusion of their background quasar in colour-colour selected samples. In order to overcome such biases, radio-selected quasar samples have been built recently: while 2001 (Ellison) did not discover a missing population, a more recent survey finds 4 fields (out of ~ 60) where the radio-flux selected quasars have no optical counterparts down to very faint limits (Jorgenson et al. 2006). These objects are the potential candidates of dusty DLAs obscuring background quasars.

In this paper, we investigate yet another possible signature of the dust content of DLAs. Indeed, dust in a quasar absorber will redden the colour of its background quasar. Pei et al. (1991) were the first to look for reddening of the quasar continua in a sample containing DLAs and detect reddening at 99.999% level. More recently, Murphy & Liske (2004) have used 79 DLAs from SDSS Data Release 2 to compare the slope of power laws fitting quasar continua with and without DLAs. These authors found a colour excess due to Small Magellanic Cloud type of dust of reddening $\langle E(B-V) \rangle < 0.01$ mag. Using colour excess measurements for SDSS sightlines containing DLAs and matching sightlines without them, Vladilo et al. (2008) report a detection of reddening in a sample of DR5 SDSS QSOs towards sightlines containing DLAs at the mean level of $\langle E(B-V) \rangle \sim 6.3 \times 10^{-3}$. They derive their estimate by comparing colours of QSOs with intervening DLAs to the mean colour of a set of QSO of similar emission redshift and brightness, and bootstrapping the resulting broad distribution of colour excesses to ascertain the slightly redder colours of the DLA QSOs. A byproduct of the Pontzen & Pettini (2009) work, who performed a Bayesian analysis on a variety of optical and radio datasets to determine the loss fraction of QSOs due to dust obscuration, is an

estimate of the probability density distribution for dust reddening in optical spectra, that also peaks around the same value for $\langle E(B-V) \rangle$. Here, we build composite spectra of quasar spectra with DLAs from SDSS Data Releases 5 and 7, and compare them with reference composite spectra built to match the original spectra in magnitudes and redshifts.

The organisation of the paper is as follows : after the introduction, we describe the selection of the DLA samples in section 2, followed by the construction of the matching non-absorber samples, and the procedure for obtaining composite spectra in section 3, where we also presents the method for deriving extinction as well as the results for the full samples. After discussing subsample analyses (section 4), we summarise and conclude in section 5.

2 DLA SAMPLE SELECTION

We start the selection of our samples from two lists of SDSS surveys for DLAs.

Prochaska & Wolfe (2009) searched in Data Release (DR) 5, following a partially automated procedure tested on earlier data releases (Prochaska & Herbert-Fort 2004; Prochaska et al. 2005). Their cleanest (‘statistical’) sample contains 738 DLAs. We have chosen not to include objects that are listed in their non-statistical sample, as these can be towards QSOs with strong intrinsic absorption, or have $z_{abs} \sim z_{QSO}$. Broad absorption line QSO (BALs) are known to be more strongly reddened in the rest-frame UV than non-BAL QSOs, and hence this list of DLAs is then cross-correlated with the BAL catalogue of Gibson et al. (2009), in order to avoid such BALs entering our analysis. Furthermore, we have restricted ourselves to those sightlines towards QSOs in the Prochaska & Wolfe (2009) sample that only exhibit one single DLA. Thus, we exclude the 59 respectively 5 cases, where two or three DLAs are found along the same line of sight. This leaves us with a sample of 526 SDSS DR5 QSO sightlines with securely identified DLA well suited for the analysis of their dust content.

Noterdaeme et al. (2009) have surveyed DR7, and present a list of 1426 strong HI absorbers at redshifts $2.15 \leq z \leq 5.2$, of which 937 systems have $\log N(\text{HI}) \geq 20.3$. Applying the same criteria for filtering out potentially problematic sightlines as above, we arrive at 731 SDSS DR7 QSO sightlines for this DLA sample.¹

While both lists have a substantial overlap (371 of Prochaska’s sources appear also in the Noterdaeme list, albeit 31 of these are estimated there to fall below the $\log N(\text{HI}) \geq 20.3$ criterion), the two methods for finding DLAs differ significantly enough to warrant keeping both datasets separate. It should, however, be kept in mind that the two samples are not independent from each other. Note also that the SDSS treatment of spectroscopic calibration has improved

¹ The BAL catalogue can only exclude objects that were already in DR5. Noterdaeme et al. (2009) make an effort to clean their samples of such sightlines, but we nonetheless found 44 entries with a match in the Gibson et al. (2009) catalogue. Hence, we also visually inspected our final sample of new DR7 sightlines to exclude obvious BALs, but found none.

from DR5 to DR7, especially the spectrophotometric algorithms. Therefore, we have decided to strictly use only the versions of the spectra that have been processed by the DR7 pipeline.

Figure 1 shows the distribution of both samples in QSO emission redshift and the i band magnitudes. In addition, we show the underlying SDSS QSO lists (cleaned of BALs and the DLAs from both lists, as detailed below) from which we can draw our matching spectra. The insert shows the histogram of the absorber redshifts for the two samples. The vast majority ($> 75\%$) of the DLAs are in the redshift range $\sim 2.2 \leq z_{abs} \leq 3.3$.

3 PROCEDURE FOR DETERMINING EXTINCTION

There are a variety of different methods to derive estimates for the reddening of each QSO spectrum, or the average reddening of the whole sample (e.g. Pei et al. (1991); Ellison et al. (2005); Richards et al. (2003); Murphy & Liske (2004); Vladilo et al. (2008). We follow closely the suggestion of York et al. (2006) and Vanden Berk et al. (2008), who have analysed the dust reddening in MgII absorbers towards SDSS QSOs. The basic principle is to define a sample of QSOs, where for each DLA quasar in question a close match in both emission redshift and i -band magnitude (and hence absolute i -band magnitude) is found, that does not contain a DLA. As York et al. (2006) point out, this matched non-absorber QSO spectrum will be of very similar data quality and hence sensitivity to similar levels of absorption at each wavelength, because of the regulation of exposure levels directly at the telescope and the exposure level check of all SDSS spectra before they are admitted to the database.

Given that there is a dispersion in the spectral slopes of QSO of similar magnitude and redshift, and hence a difficulty in matching spectra one by one, the strength of the method proposed here relies upon averaging over an as large as possible set of QSOs with individually different slopes to obtain a robust measure of the (geometric) *mean* spectra for both the samples of QSOs containing DLAs and those free of DLAs. SDSS provides for both the largest homogeneous samples of DLAs as well as the largest reservoir of QSOs from which to draw comparison spectra.

3.1 Constructing the non-absorber sample

To find an appropriate match for a DLA-containing QSO spectrum, we search the SDSS DR5 database² after cleaning it from BALs and also the DLAs found

² Currently, the catalogue of Gibson et al. (2009) only allows us to derive BAL-free samples up to DR5. Hence, we have to restrict ourselves to finding matches in DR5 only, as a reliable BAL search is beyond the scope of this paper. We have, in fact, checked for the effects of possible BAL inclusion by comparing samples drawn from DR5 strictly to those drawn including 'pure' DR7 QSOs, and concluded that indeed they lead to substantially 'redder' matching composites. Note that both the DR5 and DR7 DLA samples rely upon a BAL removal (Prochaska & Wolfe 2009;

in both lists. This resulted in a pool of 8371 QSOs with redshifts $2.24 < z_{em} < 5.31$, from which to draw the comparison spectra. We minimise the difference of the match to the QSO in the two-dimensional parameter space of the i magnitude³ and emission redshift, defined as $D^2 = (\frac{\Delta z_{em}/z_{em}}{0.007})^2 + (\frac{\Delta i}{0.08})^2$. Note that we have corrected the i magnitudes in each case for Galactic reddening. The normalisation factors in the distance metric were chosen such that the number of outliers in both quantities are minimal, as detailed in the following paragraph.

Figure 2 shows the distribution of deviations between the DLA containing spectra and their best matches in redshift and brightness for the two samples. The shape of the brightness distribution of the quasars in SDSS within the redshift range probed here, introduces a systematic Malmquist bias : in general there is a slightly higher chance to select a *fainter* match at *higher* redshift. This effect is particularly pronounced in the brightest DLA QSOs, because the number of potential counterparts below i mag ≤ 18.0 becomes too low to select an adequate match. Hence, we decided to exclude all DLA sightlines from the following analyses that deviate more than 0.08 in i mag and/or 0.007 in relative redshift difference (dotted lines in the two panels of 2). This reduces the DR5 sample to 475, and the DR7 sample to 676 DLAs. The mean i band magnitude difference Δi (DLA - match) for these is -0.0029, and -0.0022 mag, whereas the mean relative redshift differences are Δz (QSO - match)/ $z = 9.3 \times 10^{-5}$, and 5.3×10^{-5} .

In principle, we could increase the number of matches for each DLA spectrum to more than one counterpart. However, the gain in S/N (or reduced scatter) for the ratio of DLA/match, dominated then by the DLA composite's noise, which cannot be reduced, does not compensate for the loss in matching precision : the more matches are being culled from the pool, the more severe the bias becomes. Of special importance here are they increasing redshift differences that may distort the precision at which the composite match spectrum reproduces the shape of the Hence, we have decided to utilise only the best match in each case.

3.2 Constructing composite spectra

The redshift distribution for the DLA systems in conjunction with the SDSS spectral coverage ($3800 \text{ \AA} \leq \lambda \leq 9500 \text{ \AA}$) allows in principle the construction of a composite spectrum in the DLAs' restframe from $\sim 600 \text{ \AA}$ to $\sim 3000 \text{ \AA}$. Obviously, however, the flux distribution of each QSO blueward of 1215 \AA in the quasar restframe is strongly suppressed due to the neutral H column densities sampled inside the forest, in a manner specific to each sightline differently. Hence, in order to reliably determine the effects of

Noterdaeme et al. 2009), and hence it is mandatory to implement such a check for BALs into the matching strategy, as well.

³ We have used the values for the psf 'target' magnitudes and Galactic dust reddening as well as the QSO redshift SpecZ listed in the QSOConcordanceAll DR5 and DR7 datatables.

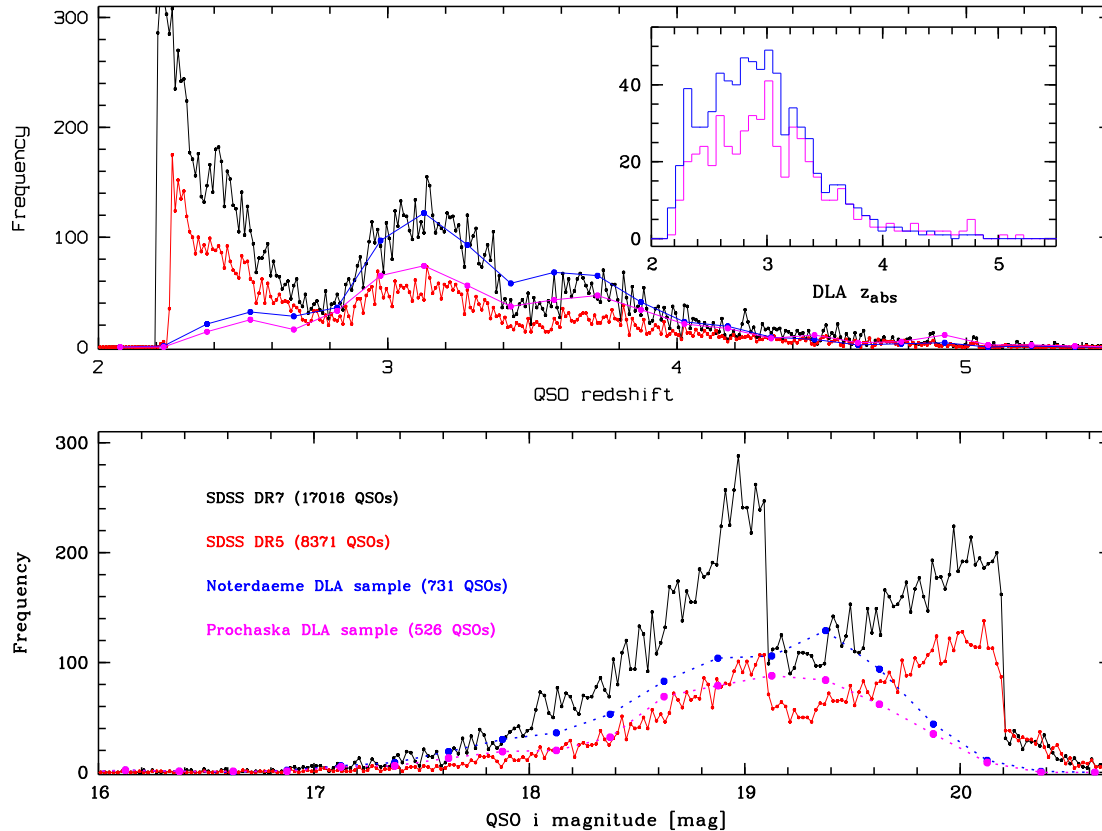


Figure 1. The distributions of the two DLA sample sightlines in QSO emission redshift and the i band magnitudes. Plotted are also the distributions for the underlying SDSS DR5 and DR7 QSOs. Note the factor 2 increase of sources from DR5 to DR7. The decrease of DLA containing sightlines towards lower redshifts, despite an increasing number of QSOs, is due to the ever shorter pathlengths over which HI absorption can be identified for the spectroscopic coverage of the instrument trailing off at 3800 \AA on the blue side. In these, and the following figures, we have corrected the observed magnitudes for Galactic reddening. The insert shows the histogram of the absorbers in both samples. The majority of DLAs (80%) are located between $2.3 \leq z \leq 3.3$. The shape of this distribution directly affects the length of the leverage arm in the DLA restframes that is at our disposal in the composite spectra.

dust reddening by comparison with an unreddened continuum, we have to restrict ourselves in each spectrum to the part redward of the beginning of the Lyman forest. We have therefore chosen to exclude all pixels in a spectrum that lie below 1240 \AA in the QSO restframe. This introduces a cutoff in the restframe of the absorbers that varies from spectrum to spectrum individually depending on the combination of z_{em} and z_{abs} .

Geometric mean spectra were then generated from the absorber and non-absorber sample in the following manner : we extend the SDSS wavelength grid with a stepsize of 0.001 in $\log \lambda$ to the lowest wavelengths covered by the spectra in the DLA restframe, and, as specified above, redward of the Lyman forest of the QSO itself. For each wavelength data point $\lambda_{DLA,RF}$ in this grid we compute for each sightline separately which pixel in the original spectrum comes to lie closest when transforming by division through the absorber redshift, i.e. we take the nearest integer value of

$$N = (\log(\lambda_{DLA,RF}(1.0 + z_{DLA}) - \log \lambda_{start}) / 0.0001 \quad (1)$$

where λ_{start} denotes the wavelength of the first pixel in each spectrum, z_{DLA} is the absorption redshift of the DLA, and N is the pixel number starting from the blue end of the

spectrum. Before computing the geometric mean of the flux distribution in the sample of the thus determined pixels, we clear it of those individual pixels flagged by the spectroscopic pipeline as possibly corrupted (Stoughton 2002). We have made no attempt in masking additional pixels, e.g. at the location of known absorption at different redshifts than the DLA. There is also no weighing of pixels according to e.g. S/N, as this possibly distorts the power-law nature of the combined spectrum. We have corrected the individual spectra for Galactic reddening (Schlegel et al. 1998). The geometric mean composite spectra for the non-absorber sets were generated in exactly the same way, using the redshift of the corresponding DLA in each case for equation 1. Note that we use in each case the spectra delivered by the DR7 pipeline, which includes the latest version of the spectrophotometric calibration. The advantage of the *geometric* mean is that it yields a meaningful average of the extinction at each wavelength by essentially averaging optical depths.

Note that our method does not rely upon any interpolation of the original spectra - at the price of sacrificing spectral resolution, because we bin together flux values

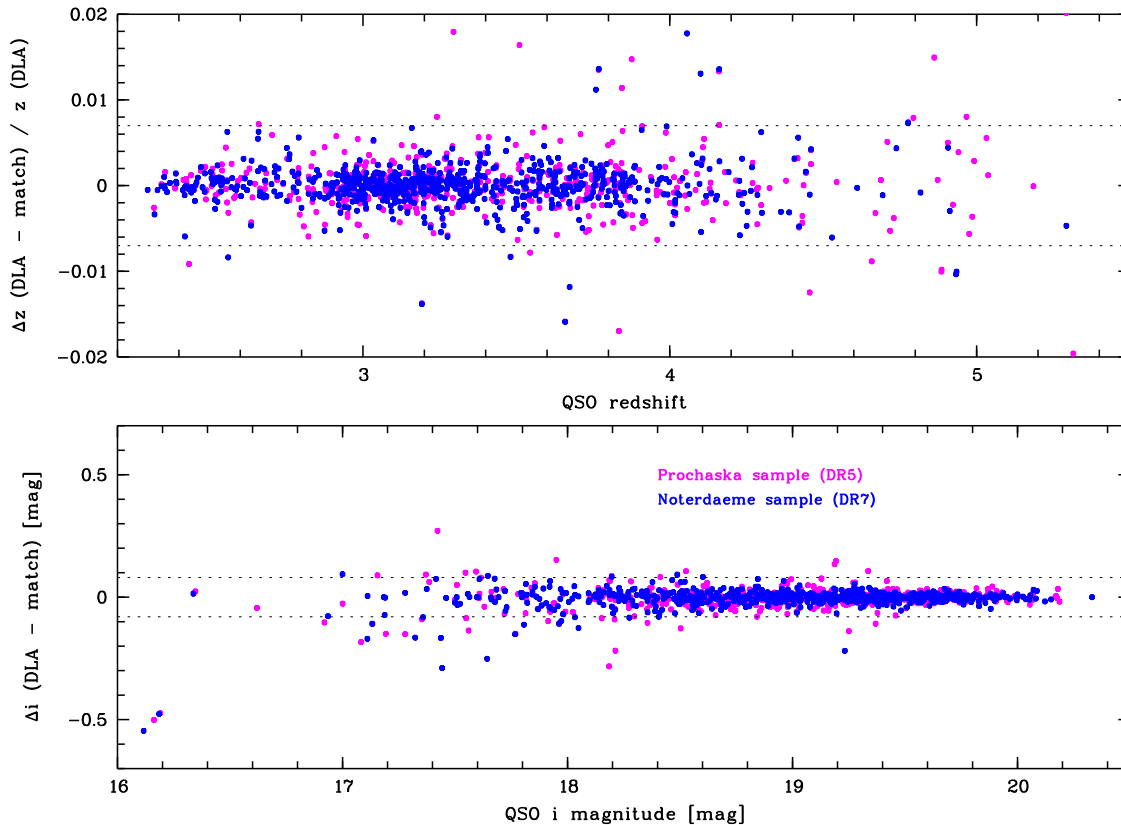


Figure 2. The difference in i band magnitude and relative z_{em} emission redshifts of the QSOs with DLAs and their matches for the DR5 (cyan) and DR7 (blue) samples. Note that there is a bias to pick fainter sources as matches, which is especially pronounced towards the brighter objects (i mag ≤ 18.0), where the number of QSOs rapidly dwindles (cf. figure 1). The dotted lines indicate the location of the boundaries that we deem acceptable for a good match.

that may reside in the DLA restframe separated by $1/2$ of a pixel at the extreme. We have tested the effects of this by comparison of the resulting composite spectra to two cases of a more refined treatment : I. rebinning each spectrum after deredshifting it, and II. computing the weighted average of the flux values of the two pixels in the original spectra that always straddle one wavelength element in the new DLA restframe grid. As expected, the differences over large wavelength ranges are negligible, and manifest themselves to a noticeable degree only on a two to three pixel scale. Hence, we believe our method, being as close as possible to the data, is robust enough not to have to rely on the intricacies of interpolation as in case I. Because we have to throw out pixels with fluxes $f_{\lambda} \leq 0.0$, method II from above results in having to flag out twice as many datapoints, which is therefore deemed less acceptable despite the higher spectral resolution.

Figure 3 shows the number of spectra contributing to each wavelength bin for the construction of the composite spectra in the DLA restframe. It also highlights to which location in these spectra the observed central wavelength of the i band (7481 \AA) is shifted in the DLA frames. Furthermore we have indicated the average brightness of the QSOs contributing at each wavelength, and the average DLA absorber redshift. Note that the region covered by

the bulk of the spectra extends from ~ 1400 to $\sim 2300 \text{ \AA}$, and exhibits fairly constant values of the mean brightness and absorber redshifts. The need for staying redward of the Lyman α emission, and the decreasing high (restframe) wavelength with increasing redshift of each QSO, result of course in fewer spectra contributing to the composite towards the edges of the wavelength regime covered by our samples. Hence, these spectral areas carry less weight due to their increased noise/scatter in the reddening analyses (as detailed in 3.3.).

3.3 Derivation of extinction

The geometric mean composite spectra of the 475 (DR5) and 676 (DR7) absorber spectra, and the corresponding non-absorbers are shown in the top panel of Figures 4 and 5. Note how the QSOs' emission lines for both samples are equally smeared out due to the different shifts applied for each specific combination of z_{em} and z_{abs} , whereas only for the DLA sample the narrow absorption lines appear in the expected places. Because of the lower numbers of spectra contributing to each wavelength bin towards the blue and red end of the composite, the noise (or scatter) starts to increase. The rise of the mean flux towards the red side is an effect of the QSOs contributing to this part of the

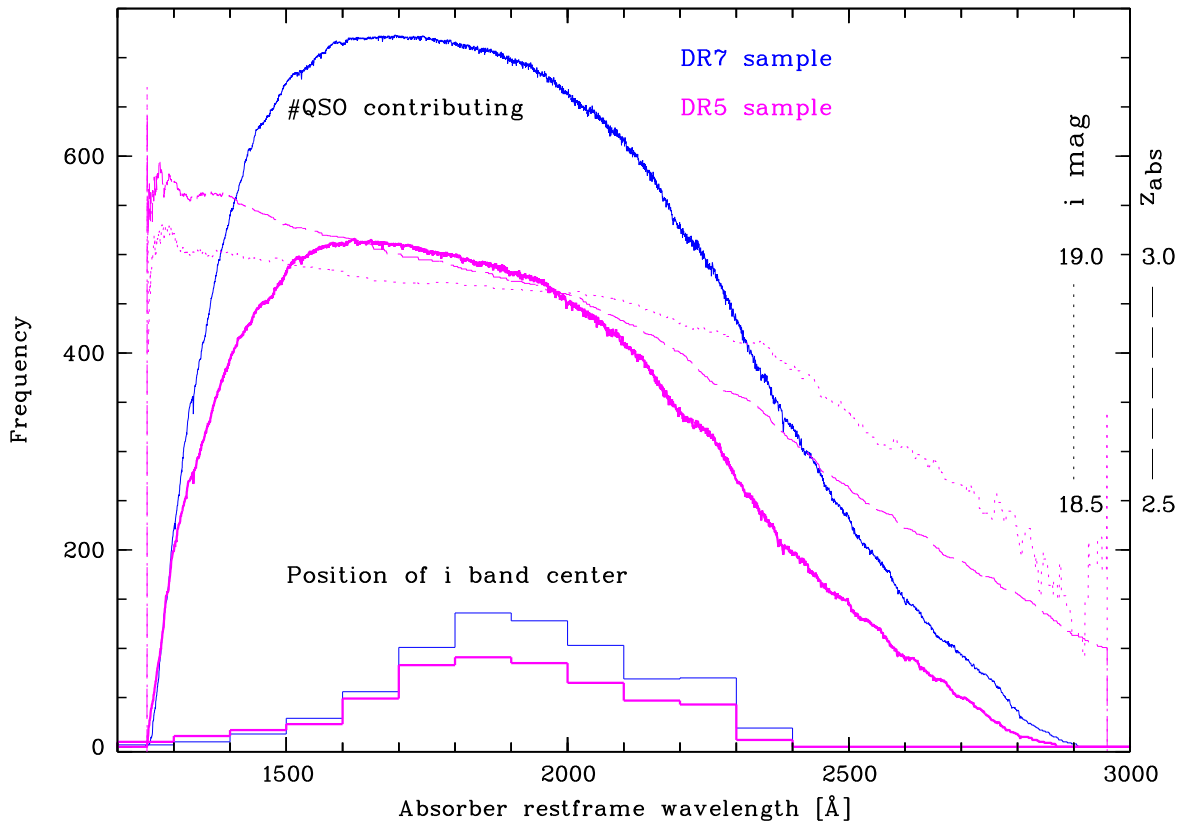


Figure 3. The number of spectra contributing to each wavelength bin for the construction of the composite spectra in the DLA restframe (solid, thick lines). Also shown is the histogram of the position of the central wavelength of the *i* band (7481 Å), that is used to find matches (frequency scale units for the histogram on the right). The dotted line marks the average brightness of the QSO sample going into the composite at each position (see scale on right axis), and hence explains the rise towards long wavelength. This is accompanied by a similar drop in the average absorber redshift (dashed lines).

spectra being on average of lower redshift and brighter (cf. Figure 1). Additionally, the abrupt change in the flux beyond 2800 Å can be attributed to the stack becoming essentially the average of a very few spectra from this point on.

The lower panels of Figures 4 and 5 show the ratios of the two composite spectra. The cyan dotted line indicates the ratio expected assuming an extinction of $\langle E(B-V) \rangle = 0.01$ for an SMC curve (Pei 1992), and represents the upper limit on $\langle E(B-V) \rangle$ derived by Murphy & Liske (2004). It is immediately obvious that very little room is left for the signature of *any* dust extinction in the DLA sample. We can quantitatively assess how much extinction can be tolerated by our data with the following procedure.

Suppose an unknown DLA stacked spectrum, $f_{DLA,nr}(\lambda)$ is reddened by dust within the absorbers, $f_{DLA,r}(\lambda)$. Then, the ratio of these two spectra would simply yield the extinction : $r_0(\lambda) = f_{DLA,nr}(\lambda)/f_{DLA,r}(\lambda) = 10^{0.4A_\lambda}$. The underlying assumption for our method is that the stacked spectrum of the matches is a good representation of the unreddened DLA stack. Our matching scheme, however, leads us to an unreddened spectrum $f_{match,nr}(\lambda)$, that, by definition, has the same flux as the (supposedly) dust reddened DLA spectrum at some fiducial wavelength

λ_0 . Hence, the ratio of the two composites in this case is modified by the extinction A_{λ_0} at this matching wavelength

$$\begin{aligned} r_1(\lambda) &= f_{match,nr}(\lambda)/f_{DLA,r}(\lambda) \\ &= 10^{0.4 \times (A_\lambda - A_{\lambda_0})} \end{aligned} \quad (2)$$

Given an extinction law, the ratio becomes a function of $E(B-V)$ only : $r_1(\lambda) = r_1(E(B-V))$. Here, we have chosen the SMC extinction curve of Pei (1992), and assume an $R_V = 2.93$ as typical for the total-to-selective ratio. Note that the choice of the SMC reddening curve is the most constraining regarding the absence of dust signatures - LMC or even MW dust type induces stronger reddening. Because we are fitting the slope of this function, the potential offsets in A_{λ_0} are of no relevance in this circumstance, and hence the normalisation of the ratio curve is not important.

Figure 6 shows the results of these one-parameter fits for DLAs (this work) and two SDSS samples of MgII absorbers (York et al. 2005; Vanden Berk et al. 2008). To obtain the latter two, we have applied exactly the same averaging scheme as outlined above. Before the calculation of the goodness of fit statistic, χ^2/ν (where ν denotes the degrees of freedom for the fit), we have taken out areas of ± 5 Å from the known, narrow metal lines in the

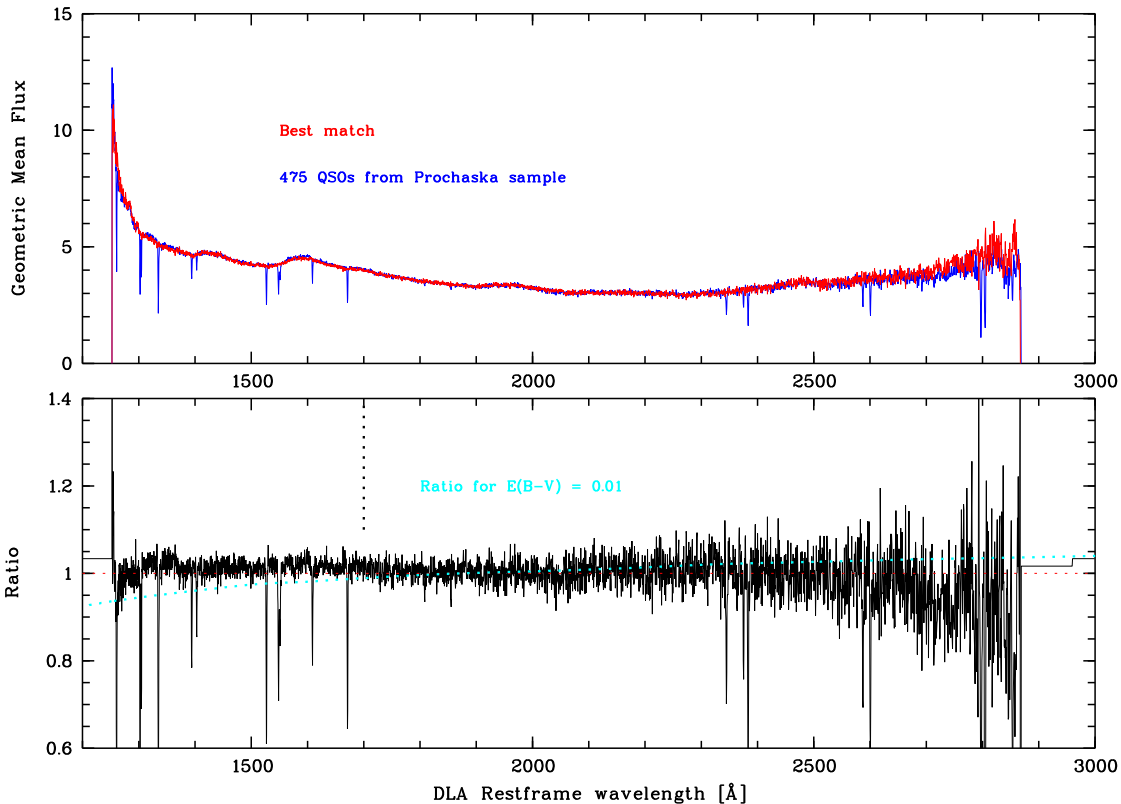


Figure 4. Upper panel: The composite restframe spectra of the DLA DR5 sample (blue) and the corresponding sample of best matches (red). Before averaging the spectra, as detailed in the text, a Galactic dust extinction correction is applied. The stretched out broad emission lines have very similar shapes, indicating the suitability of the match for the analysis at hand. Only the DLA composite exhibits narrow metal line absorption features. The rise of the curves towards the red end is purely an effect of the larger average brightness of the sources at lower redshift, which are the sole contributors at this wavelength regime (cf. Figure 1). **Lower panel:** Ratio of the two composite spectra from the upper panel. The cyan dotted line indicates the ratio expected for an SMC extinction with $E(B-V)=0.01$ (Pei 1992), which exhibits clearly much more curvature than the data allow. The black dotted vertical line at 1700 Å indicates the position bluewards of which the strong emission lines of CIV, possibly with contributions from Fe lines, and SiIV render the exact matching of spectral shape increasingly difficult (see text for details).

spectra. We find that we can constrain the amounts of extinction for those two samples of MgII absorbers very tightly : $\langle E(B-V) \rangle = 0.012 \pm 0.002$ for the intervening, and $\langle E(B-V) \rangle = 0.025 \pm 0.003$ for the associated cases. We therefore reproduce the results of York et al. (2005) and Vanden Berk et al. (2008) well, despite the fact that we do not explicitly also remove regions of the spectra that are affected by strong absorption at redshifts different from the MgII absorbers. We take this test as a sign that both our stacking algorithms and the method to estimate the reddening are robust and accurate for these MgII samples. We note, however, that the lower redshift of these absorbers (compared to our samples of DLAs) may reduce the problem of the foreground reddening due to the lower redshift path sampled, and the intrinsically lower density of absorbers in the low- z universe.

We have also applied this spectral method to the samples of DLAs and ‘pool’ QSOs used by Vladilo et al. (2008) for their photometric analysis. These authors have taken care to take out QSOs that may be afflicted

by absorption unrelated to the DLAs. Again, we are able to reproduce their results very well, and derive an $\langle E(B-V) \rangle = 6.2 \pm 1.8 \times 10^{-3}$, indicating that both methods yield similar results when applied to the same samples. Here, the strength of our method is specifically that all the unrelated effects will affect both the DLA and the pool spectra in the same way, and hence we choose to increase the sample size to ensure that these effects are averaged out. We are making use of both the largest databases for DLAs *and* comparison spectra (increasing the number of DLAs by almost a factor of 3 for the DR7 sample, and the number of the objects in the comparison pool by a factor of 5 compared to the Vladilo samples).

A word of caution is necessary when trying to quantify the confidence intervals for our results. Nominally, the number of degrees of freedom (d.o.f.) for the two samples are 2543 (DR7) and 2583 (DR7), after taking out the pixels affected by metal-line absorption, and restricting ourselves to the wavelength region below 2500 Å to avoid the large drop in both numbers of spectra contributing and average

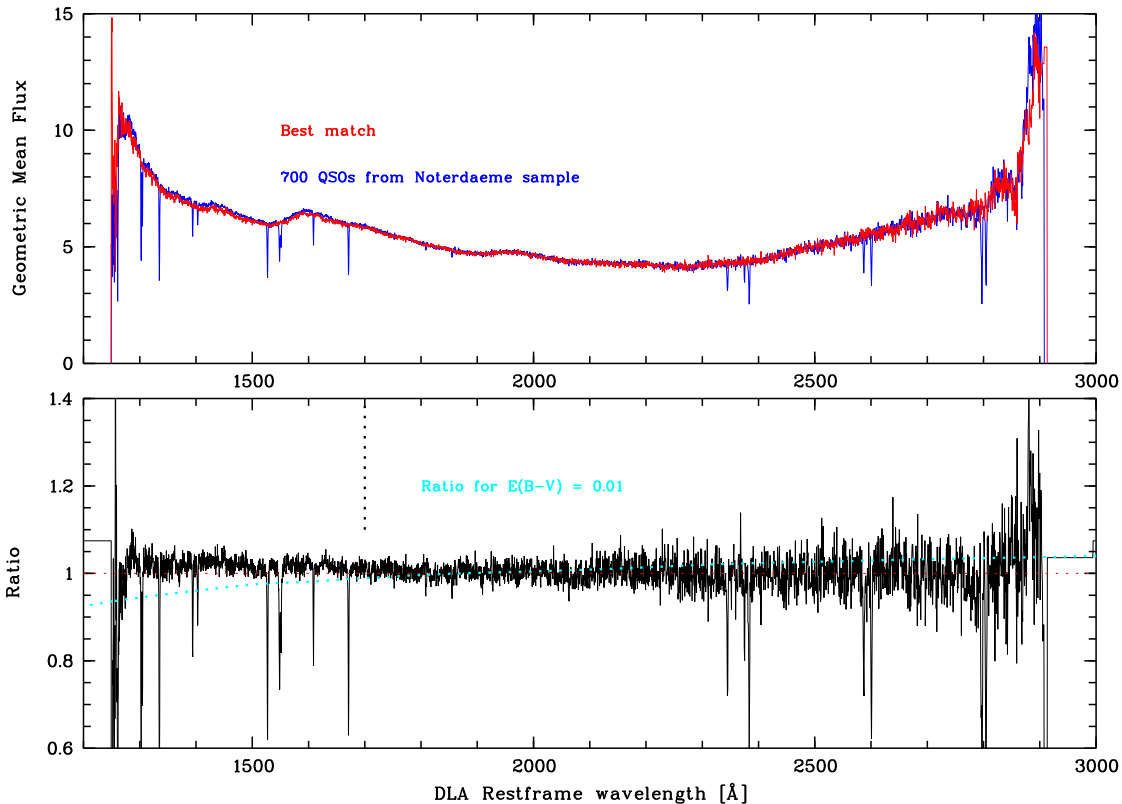


Figure 5. Same as figure 4 for the DR7 sample.

QSO brightness. However, as we have detailed in the section on the construction of the composite spectra, adjacent pixels are not truly independent of each other. We have tested the robustness of the fits by binning the composites (with bin sizes up to 5 pixels, hence reducing the d.o.f. by the same factor). Hence, we arrive at measurements of the mean $\langle E(B-V) \rangle = -0.0013 \pm 0.0025$ (DR5) and $\langle E(B-V) \rangle = -0.0017 \pm 0.0022$ (DR7) for the full samples⁴, where the error budget adopts a generous 3σ level for the approach with the 5-pixel bin.

In order to test whether we could have detected an $\langle E(B-V) \rangle$ distribution as predicted by Pontzen & Pettini (2009) and measured by Vladilo et al. (2008), we have artificially reddened each DLA quasar spectrum by a value drawn from a lognormal distribution of width 0.4 dex and mean of $\log \langle E(B-V) \rangle = -2.2$, broadly consistent with those two studies. Figure 7 shows that we not only could clearly detect such a reddening, but also could retrieve the input value very accurately (red curve in Figure 6). In fact,

⁴ Of course, negative reddening values are per se unphysical, but the natural outcome of the fitting routine. These are largely driven by the fact that the regions in the spectrum with the strong QSO emission lines between 1300 and 1700 Å cannot be expected to be perfectly matching, given the complicated line emission structures of quasars. This difficulty, and not sample size, probably also sets the limiting precision of our method.

the two χ^2 curves for our spectral analyses and the fake reddening are excluded by several σ .

We have also performed a 'null test' by comparing the composite spectra of the matched samples with composites created from the samples of the 2nd best, 3rd best, etc... matching samples. As expected, the analysis of the ratios of these stacked spectra yields no detectable reddening, and the range of $\langle E(B-V) \rangle$ values obtained by this procedure ranges from $-0.002 \leq \langle E(B-V) \rangle \leq 0.002$ for DR5, and $-0.0018 \leq \langle E(B-V) \rangle \leq 0.001$ for DR7. Hence we encompass the two measurements with the DLA samples. We note in passing that the main difficulty in matching the shape of the composites and their comparison counterparts lies in the strong emission lines of the QSOs, especially blueward of ~ 1700 Å, where the Fe-complexes have a profound influence on the flux above the continuum. Indeed, when inspecting the ratio curves for the two samples, around that wavelength there seems to appear a 'kink' in them, which may be caused by a mismatch in the emission lines. This is the main driver towards these (very low) 'negative' $\langle E(B-V) \rangle$ values we obtain formally from the fitting. If we restrict ourselves to either the ratios blueward or redward of this feature, the fitting results in exact null values (at the expense of leverage in wavelength).

One possible complication in matching the quasars' luminosities based upon their emission redshifts and the ob-

served i band magnitudes is that the latter could systematically underestimate the true continuum flux for the DLA sample compared to their non-DLA counterparts because of a higher fraction of strong metal absorption lines due to the presence of the DLA. A rough estimate of the size of this effect indicates that in sightlines where a very strong absorber (of the order of 5 Å restframe equivalent width) is present in the i band, it will result in a photometric measurement that is decreased from the 'normal' QSO brightness by 2%. Thus we may in such cases be selecting QSOs as matches that are systematically too faint. We have tested whether such a possible bias may influence our analysis of the dust reddening signal by creating samples of matches following exactly the procedures described above, but introducing an artificial offset δi in the i band magnitude by minimising $\Delta(i_{DLA} + \delta i) - i_{match}$. Even shifts as large as $\delta i = -0.2$ magnitudes do not change the overall shape of the composite spectra, yielding almost exactly the same results for the reddening estimates when fitting for the slope of the ratio curves.

4 EXTINCTION ANALYSES FOR SUBSAMPLES

While the full samples of DLA sightlines do not show any appreciable sign of dust reddening to a high degree of accuracy, it is still possible that there are certain subsets of DLAs and/or sightlines that do exhibit an amount of wavelength dependent extinction, which is simply too small to be detected when averaging over such large datasets. In order to check for such potential trends, we have divided the DLA lists into subsamples according to various criteria concerning the DLAs themselves (namely absorption redshift, HI column density, and the ab- or presence of metal lines) or the underlying QSO sightlines (apparent brightness or emission redshift). To keep a high enough number of DLAs we have in almost all cases decided to simply split the full samples into two halves.

Figure 8 shows the results of a split (for the DR5 sample)⁵ into the highest (left panel) and lowest (right panel) HI column densities for the DLA. The mean of these subsamples are at $\log N_{HI} = 20.91$, and $\log N_{HI} = 20.42$. Clearly, there is no difference in the fact that there is a null detection for both subsamples.

Figure 11 shows how differentiating the samples according to the absorber redshifts affects the dust reddening analysis. Again, both for the low and the high redshift subsamples (mean $z_{abs} = 2.63$, and 3.39, respectively) there is no reddening detectable. Note how the higher redshift sample leads to a lower wavelength cut-off, and due to the generally fainter spectra a slightly higher noise in the composite.

Figure 10 demonstrates that the DLAs classified by Prochaska & Wolfe (2009) as containing no visible narrow

metal absorption lines in individual SDSS spectra, do also not exhibit any such signs in their composite. Only 88 of the 475 DLAs fall into this class (18.5%), and hence the noise in the composite is much higher than in the other subsamples. Yet, both classes do not show reddening.

The separation into QSOs of low and high redshifts (shown in Figure 12, mean $z_{abs} = 2.31$ and 3.78) is similar to the cut in QSO brightness (mean i band psf magnitude of $i = 18.62$, and 19.48 mag, corrected for Galactic reddening), because of the trend for fainter sources with higher redshift. The subsample with the brightest QSOs (for DR5)⁶ is the only one that does show a positive value of the colour excess, but not significantly different from a null detection : $\langle E(B-V) \rangle = 0.0012 \pm 0.0025$.

To summarise, none of these simple subselections do give rise to the assumption that there are significant trends in reddening regarding either the observational constraints (brightness and emission redshift of sources) or DLA properties (absorption redshift, additional narrow metal line absorption, and HI column density).

5 SUMMARY AND CONCLUSIONS

While our analysis technique reproduces well past results for other classes of absorbers at different redshifts (Vanden Berk et al. 2008; York et al. 2006), and DLAs using other methods (Murphy & Liske 2004) and (Vladilo et al. 2008) where some extinction could be detected, we could not detect any significant extinction in samples of DLAs drawn from the Data Releases 5 and 7 of the SDSS. These findings are based on the largest DLA sample ever studied, but also on the largest sample of quasars from which to draw a reference spectrum. The implication is that most of the DLAs observed in SDSS have a very small dust content.

York et al. (2006) have analysed SDSS spectra with intervening strong MgII absorbers, and detect clear dust reddening. More specifically, their subsamples with the highest MgII equivalent width (subsamples 8 and 25 in their notation, Table A4) show the highest degrees of reddening ($\langle E(B-V) \rangle = 0.032$ and 0.085). These strong MgII absorbers are then classified, based on the column densities of the accompanying metal lines, as akin to low redshift DLAs. We note however, that a direct measurement of the HI absorption in these absorbers was not possible due to the low wavelength cutoff of SDSS, and the mean HI column densities for the subsamples are derived by using an SMC relationship between $\langle E(B-V) \rangle$ and HI. Rao et al. (2006) also caution that not all high EW MgII absorbers are indeed DLAs, although York et al. (2006) point out that the specific requirement of the QSOs probed by Rao et al. (2006) with HST being UV-bright introduces a bias against red QSOs, that may have led them to an underestimate of the DLA fraction. Hence, it is a priori

⁵ We have performed the subsample analyses for both DR5 and DR7, yielding the same results, but only show the results for DR5 here as examples.

⁶ The same cut in the DR7 sample does not show such a detection.

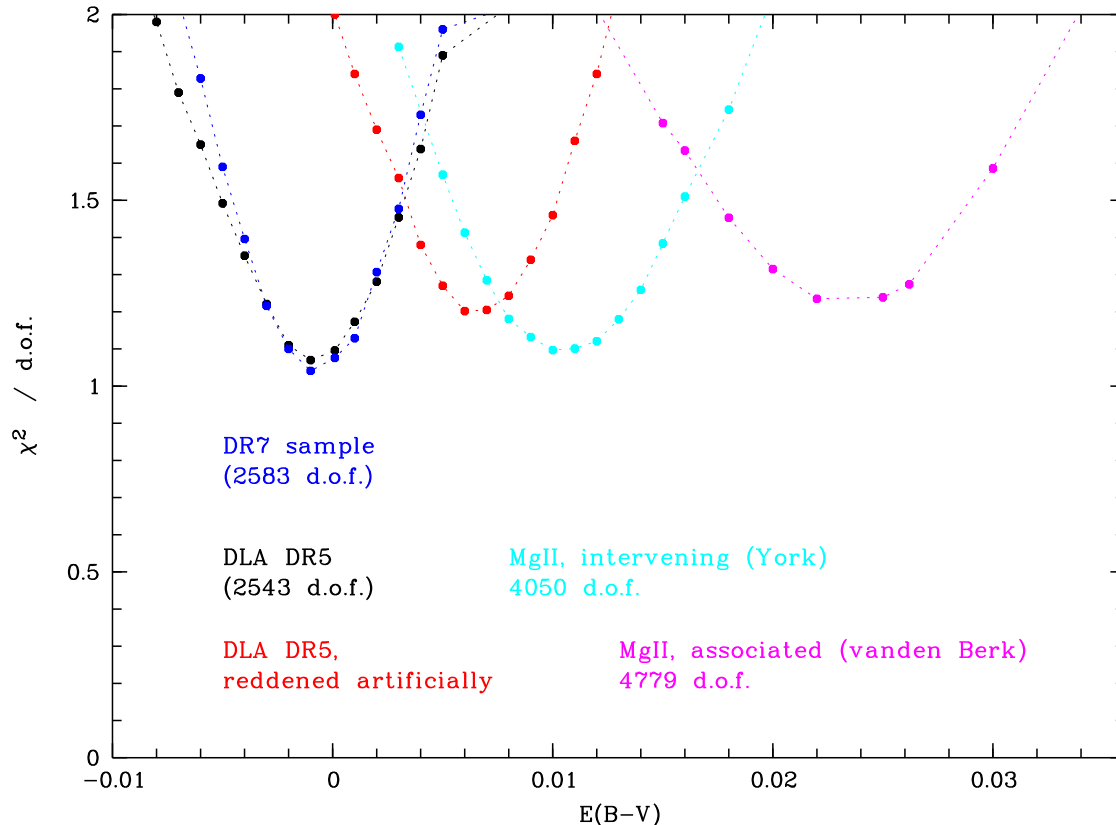


Figure 6. Results of the one-parameter fit for the dust reddening in various absorber types. Plotted are the χ^2 per degree of freedom distributions obtained by fitting the ratio of the composite spectra with a one-parameter extinction curve (for details see text). The two curves in magenta and cyan show the results for the samples of intervening and associated MgII absorbers in SDSS spectra (York et al. 2005; Vanden Berk et al. 2008). We recover the extinction $\langle E(B-V) \rangle$ measured by these authors. The black and blue curves are a result of the fit to the DLA sample. Note that we can clearly rule out any signs of extinction $\langle E(B-V) \rangle > 0.002$ with very high confidence. The curve in red shows the result for the DR5 sample that has been artificially reddened by a lognormal distribution with mean $\langle E(B-V) \rangle = 6.3 \times 10^{-3}$, which is well recovered.

not clear whether our results contradict these findings. Also note that there may be a redshift evolution effect. In fact, Ménard et al. (2008) have noted that the rest-frame colour excess $E(B-V)$ for their MgII samples shows a strong decline with increasing redshift (their figure 10, lower right panel). Thus, it is possible that the difference in the mean redshifts of our samples ($z_{obs} \sim 3.1$) compared to the lower $z_{obs} \sim 1.4$ of York et al. (2006) may partly explain the seemingly discrepant results.

Yet another strategy involving spectral analysis is fitting the QSO continuum spectra by a power-law, and checking for deviations in the slope of these for spectra with and without DLAs. Employing this technique, Murphy & Liske (2004) can place an upper limit for a sample of 70 DLAs from SDSS DR2 of $\langle E(B-V) \rangle = 0.01$. Note that we can rule out such a high value for our samples with a very high degree of confidence.

In addition, there have been claims of firm detections of dust reddening towards sightlines afflicted by intervening DLAs. Specifically, Vladilo et al. (2008) report a mean $E(r-z) = 27(\pm 9) \times 10^{-3}$ for a subsample of the same DR5 DLA

sample that we use. When applying our method to these subsamples of DLAs *and* the subsample of DR5 'pool' QSOs for the constructing of the comparison spectrum, we recover their results. Note that Vladilo et al. (2008) have removed all quasars from their samples that may have additional absorption unrelated to the DLA, reducing the number of objects in each sample by a large fraction. We conclude that the differences do not reside in the methods, but the sample selection. We note that the reddening distribution of undesired interlopers probably has a tail with a small number of objects exhibiting much larger than the typical reddening expected from DLA systems. It may hence be that for such low frequency events, that cases of e.g. BAL QSOs, despite efforts to filter them out, enter the DLA samples more often than the comparison pool, and hence could wash out the signal. Increasing the sample size reduces the possible impact of such 'special', very red QSOs.

Our result is also at odds with expectations from the evolution of high-redshift galaxies (but see Pontzen et al. (2008)). It should be emphasised however that there are two separate issues: i) what is the dust content of the quasar absorbers we know of today and ii) which fraction of the quasar absorbers are missed because of the extinction

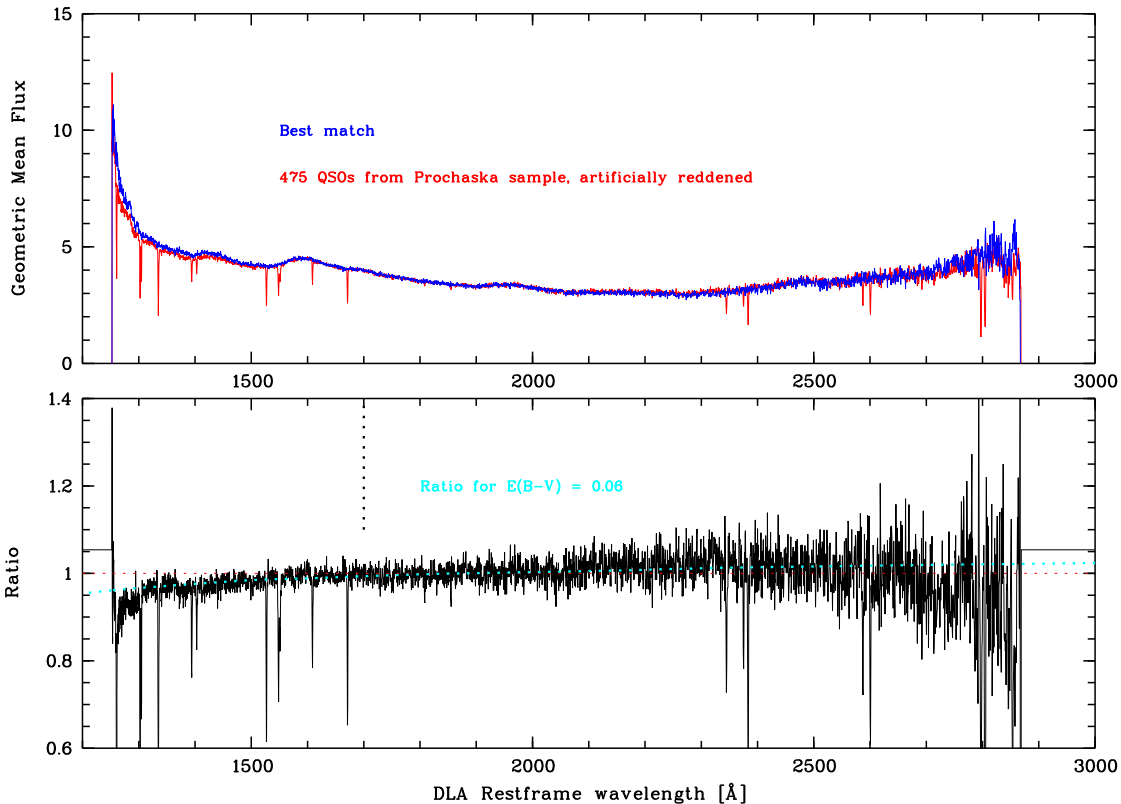


Figure 7. The result of artificially reddening the DR5 DLA sample spectra with each QSO subjected to an $\langle E(B-V) \rangle$ drawn randomly from a lognormal distribution of mean $\log \langle E(B-V) \rangle = -2.2$ and width 0.4 dex, resembling the values found by Vladilo et al. (2008) and Pontzen & Pettini (2009). The reddening is not only clearly detected by our method, but also the input value is returned accurately. Labelling and underlying comparison spectrum just like in Figure 4.

they induce on their background quasar such that it is not selected in the first place. Indeed, models of galactic chemical evolution (e.g. Prantzos & Boissier (2000) predict the existence of regions of high metallicity and column density which are mostly not detected in current DLA surveys (Boissé et al. 1998). One way to reconcile these two findings is to invoke a dust-bias in the observations. These apparent discrepancies could indeed be explained by the dust content of the absorbers themselves: they could absorb enough light from the quasar to make the latter too faint to be included in current quasar samples, which barely go beyond magnitude $g \sim 20.2$. In fact, an extension of the Fall & Pei (1993) calculations taking into account recent observations addresses both these issues: Vladilo & Péroux (2005) propose that whilst the dust content of the DLAs in current samples is not high, the missing fraction is possibly quite important ranging from 30% to 50% at $z = 1.8 - 3.0$. One way to test such a hypothesis is to look at fainter objects than what can be probed with SDSS. Using a Bayesian analysis of these issues in light of different techniques and datasets Pontzen & Pettini (2009) posit that probably less than 10% of DLAs have been missed in current optical samples, and also derive an $\langle E(B-V) \rangle$ posterior probability distribution peaking strongly around $\log \langle E(B-V) \rangle \sim -2.0$.

On the other hand, if the absence of the detection of extinction in DLAs is not due to an observational bias, then selecting in absorption implies that we are picking a population of high-redshift galaxies which have probably undergone little star formation, e.g. Weatherley et al. (2005) and Wolfe et al. (2006). This is difficult to reconcile with the fact that these system are gas-rich by construction.

6 ACKNOWLEDGMENTS

This work has benefitted from support of the "Agence Nationale de la Recherche" with reference ANR-08-BLAN-0316-01. We would like to thank Bruno Milliard, Jean-Michel-Deharveng, Jochen Liske, and Michael Murphy for helpful comments refining the analysis substantially. We thank the referee for a thorough review of the results and valuable suggestions, that improved the manuscript.

Funding for the SDSS and SDSS-II has been provided by the Alfred P. Sloan Foundation, the Participating Institutions, the National Science Foundation, the U.S. Department of Energy, the National Aeronautics and Space Administration, the Japanese Monbukagakusho, the Max Planck Society, and the Higher Education Funding Council

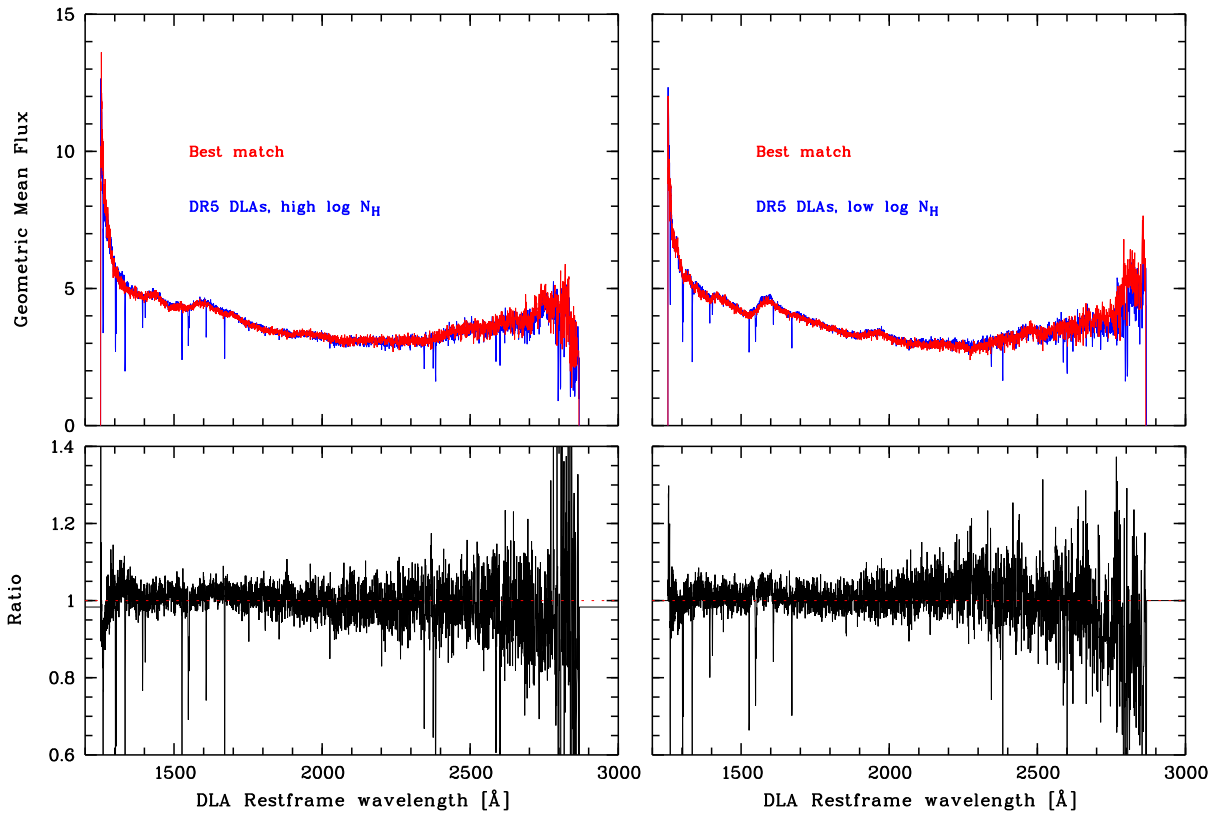


Figure 8. Comparison of the geometric mean spectra and their ratios for the subsamples with the **highest** (left panels) and **lowest** (right) column densities $\log N_{HI}$. Note that for this, and the following plots (with the exception of the metal-no metal distinction), each of the subsamples simply contains half the number of sightlines as the original full sample.

for England. The SDSS Web Site is <http://www.sdss.org/>.

The SDSS is managed by the Astrophysical Research Consortium for the Participating Institutions. The Participating Institutions are the American Museum of Natural History, Astrophysical Institute Potsdam, University of Basel, University of Cambridge, Case Western Reserve University, University of Chicago, Drexel University, Fermilab, the Institute for Advanced Study, the Japan Participation Group, Johns Hopkins University, the Joint Institute for Nuclear Astrophysics, the Kavli Institute for Particle Astrophysics and Cosmology, the Korean Scientist Group, the Chinese Academy of Sciences (LAMOST), Los Alamos National Laboratory, the Max-Planck-Institute for Astronomy (MPIA), the Max-Planck-Institute for Astrophysics (MPA), New Mexico State University, Ohio State University, University of Pittsburgh, University of Portsmouth, Princeton University, the United States Naval Observatory, and the University of Washington.

REFERENCES

- Boissé, P. & Bergeron, J. 1988, *A&A*, 192, 1
 Boissé, P., Le Brun, V., Bergeron, J., & Deharveng, J. 1998, *A&A*, 333, 841
 Chen, H., Kennicutt, Jr., R. C., & Rauch, M. 2005, *ApJ*, 620, 703
 Ellison, S. L., Hall, P. B., & Lira, P. 2005, *AJ*, 130, 1345
 Ellison, S. L., Yan, L., Hook, I. M., et al. 2001, *A&A*, 379, 393
 Fall, S. M. & Pei, Y. C. 1993, *ApJ*, 402, 479
 Fall, S. M., Pei, Y. C., & McMahon, R. G. 1989, *ApJL*, 341, L5
 Gibson, R. R., Jiang, L., Brandt, W. N., et al. 2009, *ApJ*, 692, 758
 Jorgenson, R. A., Wolfe, A. M., Prochaska, J. X., et al. 2006, *ApJ*, 646, 730
 Junkkarinen, V. T., Cohen, R. D., Beaver, E. A., et al. 2004, *ApJ*, 614, 658
 Jura, M. 1977, *Nature*, 266, 702
 Kulkarni, V. P., Fall, S. M., & Truran, J. W. 1997, *ApJL*, 484, L7+
 Kulkarni, V. P. and York, D. G. and Vladilo, G. and Welty, D. E. 2007, *ApJ*, 663, 81
 Lanzetta, K. M., Wolfe, A. M., & Turnshek, D. A. 1989, *ApJ*, 344, 277
 Ménard, B., Nestor, D., Turnshek, D., Quider, A., Richards, G., Chelouche, D., & Rao, S., 2008, *MNRAS*, 385, 1053
 Murphy, M. T. & Liske, J. 2004, *MNRAS*, 354, L31
 Nagamine, K., Springel, V., & Hernquist, L. 2004, *MNRAS*, 348, 435

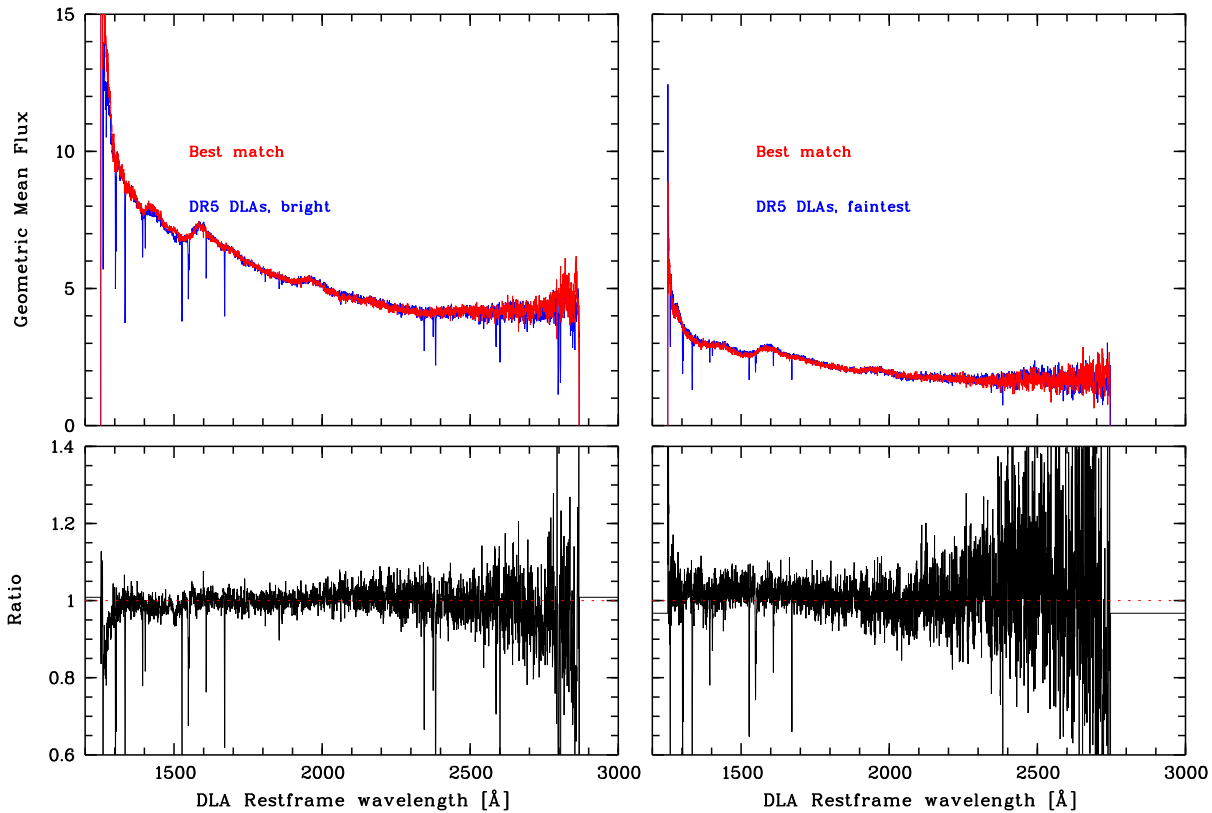


Figure 9. Comparison of the geometric mean spectra and their ratios for the subsamples with the **brightest** (left panels) and **faintest** (right) QSOs. Obviously, the ratio for the fainter subsample is noisier, yet no systematic of reddening in either subsample can be discerned.

Noterdaeme, P., Petitjean, P., Ledoux, C., & Srianand, R. 2009, *A&A*, 505, 1087
 Pei, Y. C. 1992, *ApJ*, 395, 130
 Pei, Y. C., Fall, S. M., & Bechtold, J. 1991, *ApJ*, 378, 6
 Pettini, M., Ellison, S. L., Steidel, C. C., Shapley, A. E., & Bowen, D. V. 2000, *ApJ*, 532, 65
 Pontzen, A., Governato, F., Pettini, M., Booth, C. M., Stinson, G., Wadsley, J., Brooks, A., Quinn, T. & Haehnelt, M. 2008, *MNRAS*, 390, 1349
 Pontzen, A. & Pettini, M. 2009, *MNRAS*, 393, 557
 Prantzos, N. & Boissier, S. 2000, *MNRAS*, 315, 82
 Prochaska, J. X. & Herbert-Fort, S. 2004, *PASP*, 116, 622
 Prochaska, J. X., Herbert-Fort, S., & Wolfe, A. M. 2005, *ApJ*, 635, 123
 Prochaska, J. X. & Wolfe, A. M. 2009, *ApJ*, 696, 1543
 Rao, S. M., Nestor, D. B., Turnshek, D. A., et al. 2003, *ApJ*, 595, 94
 Rao, S. M., Turnshek, D. A., & Nestor, D. B. 2006, *ApJ*, 636, 610
 Richards, G. T., Hall, P. B., Vanden Berk, D. E., et al. 2003, *AJ*, 126, 1131
 Savaglio, S., Panagia, N., & Stiavelli, M. 2000, in *Astronomical Society of the Pacific Conference Series*, Vol. 215, *Cosmic Evolution and Galaxy Formation: Structure, Interactions, and Feedback*, ed. J. Franco, L. Terlevich, O. López-Cruz, & I. Aretxaga, 65–+
 Schlegel, D. J., Finkbeiner, D. P., & Davis, M. 1998, *ApJ*,

500, 525
 Smith, H. E., Margon, B., & Jura, M. 1979, *ApJ*, 228, 369
 Steidel, C. C., Adelberger, K. L., Giavalisco, M., Dickinson, M., & Pettini, M. 1999, *ApJ*, 519, 1
 Stoughton, C. e. a. 2002, *AJ*, 123, 485
 Vanden Berk, D., Khare, P., York, D. G., et al. 2008, *ApJ*, 679, 239
 Vladilo, G. & Péroux, C. 2005, *A&A*, 444, 461
 Vladilo, G., Prochaska, J. X., & Wolfe, A. M. 2008, *A&A*, 478, 701
 Wang, J., Hall, P. B., Ge, J., Li, A., & Schneider, D. P. 2004, *ApJ*, 609, 589
 Weatherley, S. J., Warren, S. J., Møller, P., Fall, S. M., Fynbo, J. U. & Croom, S. M. 2005 *MNRAS*, 358, 985
 Wolfe, A. M. and Chen, H.-W. 2006 *ApJ*, 652, 981
 York, D. G., Khare, P., Vanden Berk, D., et al. 2006, *MNRAS*, 367, 945
 York, D. G., vanden Berk, D., Richards, G. T., et al. 2005, in *IAU Colloq. 199: Probing Galaxies through Quasar Absorption Lines*, ed. P. Williams, C.-G. Shu, & B. Menard, 58–64

This paper has been typeset from a \TeX / \LaTeX file prepared by the author.

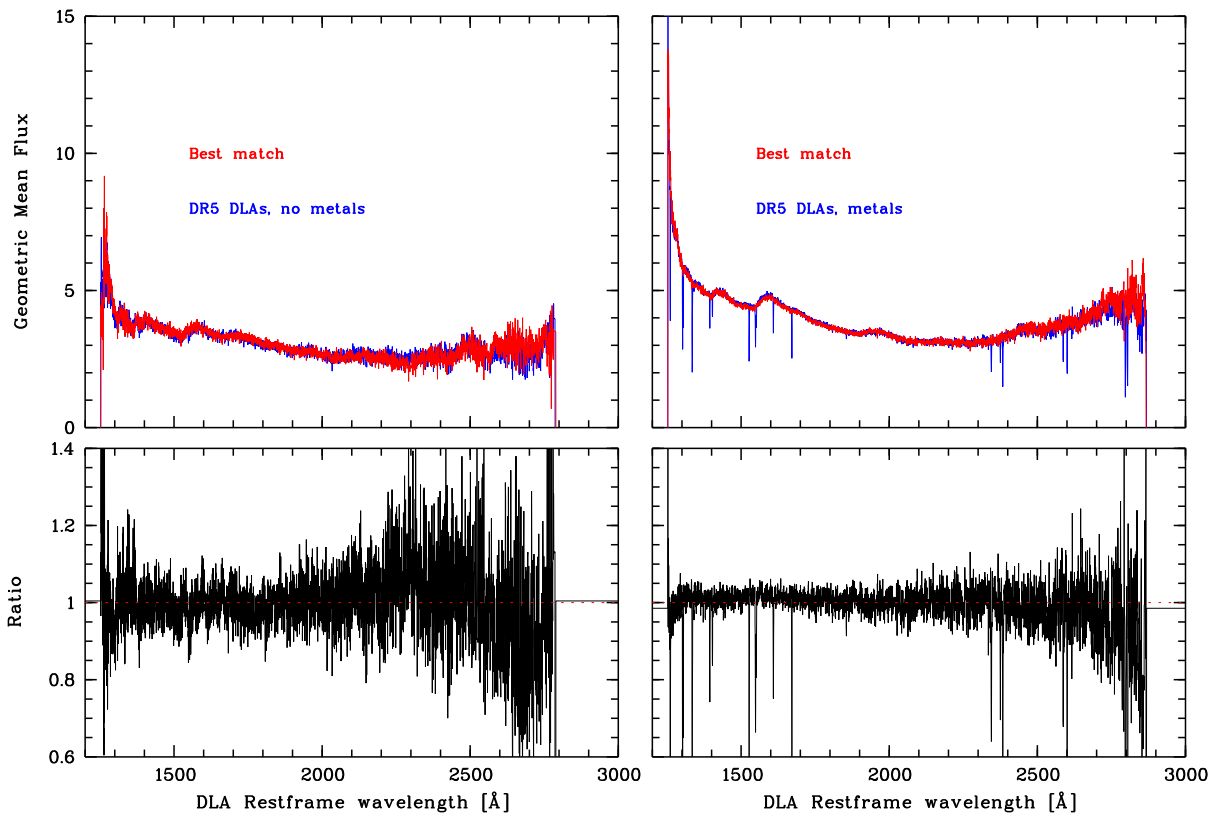


Figure 10. Comparison of the geometric mean spectra and their ratios for the subsamples with the DLA that do not exhibit sign of **metal-line absorption** (left panels, 88 DLAs in total) and the ones that do (right panels). Note the conspicuous absence of *any* sign of metal-line absorption in the DLA stack on the left.

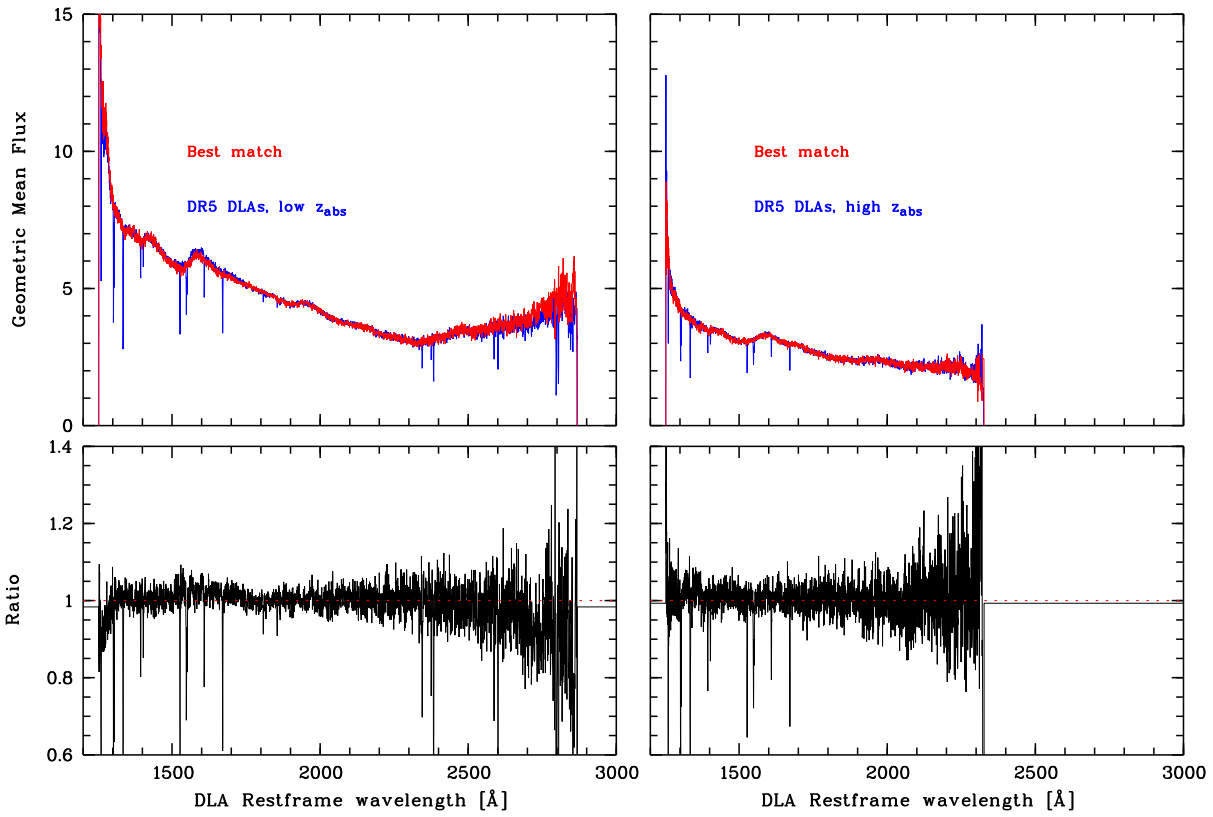


Figure 11. Comparison of the geometric mean spectra and their ratios for the subsamples with the **lowest** (left panels) and **highest** (right) DLA absorber redshifts. Notice the lower cut-off wavelength for in the DLA restframe for absorbers with higher redshifts. Despite the fact that hence the 'kink' beyond $\sim 2500\text{\AA}$ in the stacked spectrum of the low redshift subsample gets even more pronounced than in the overall sample, the matched spectrum still follows this quite accurately.

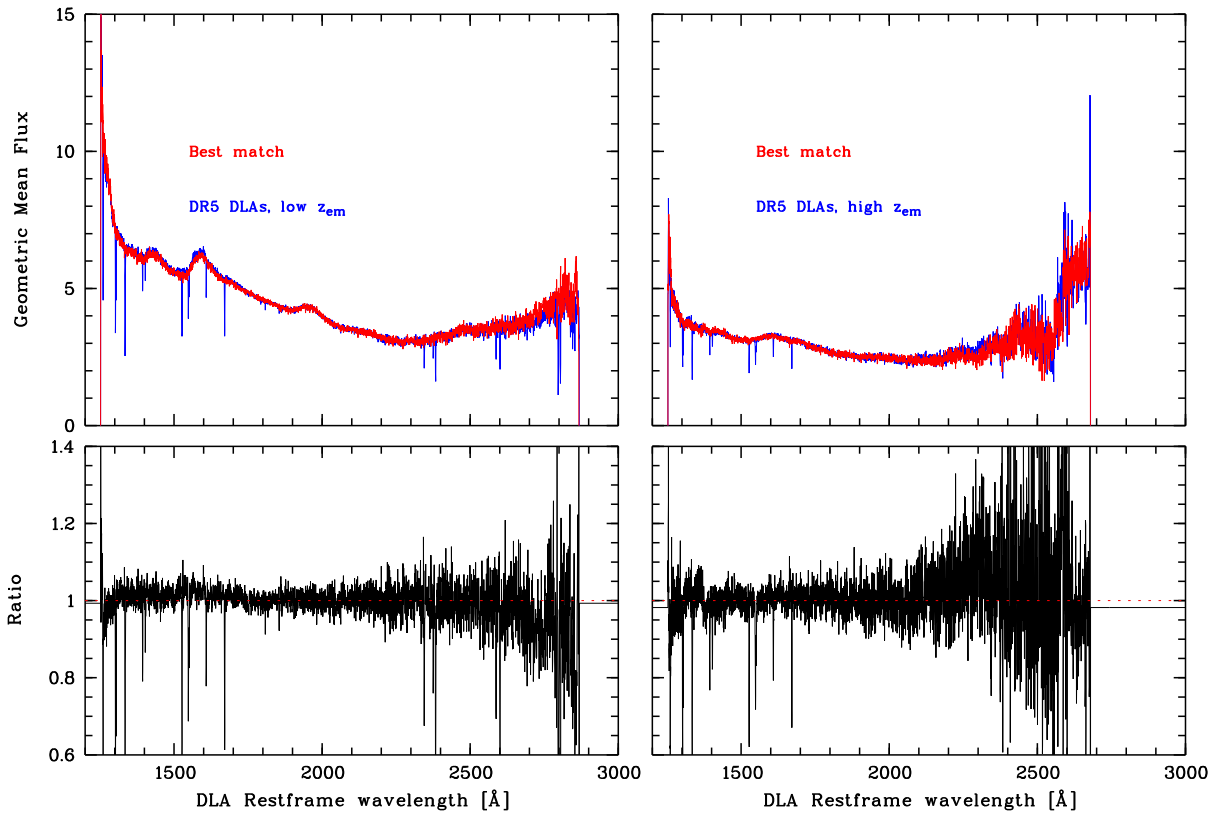


Figure 12. Comparison of the geometric mean spectra and their ratios for the subsamples with the **lowest** (left panels) and **highest** (right) QSO emission redshifts. Note the rapidly increasing noise for the high redshift subsample towards the red part of the composite. The separation into QSOs of low and high redshifts is similar to the cut in QSO brightness. The subsample with the brightest QSOs (for DR5) is the only one that does show a positive value of the colour excess, but not significantly different from a null detection : $\langle E(B-V) \rangle = 0.0012 \pm 0.0025$.